

Open access • Journal Article • DOI:10.1038/308032A0

Cryo-electron microscopy of viruses — [Source link](#)

Marc Adrian, Jacques Dubochet, J. Lepault, Alasdair W. McDowall

Published on: 01 Mar 1984 - Nature (Nature Publishing Group)

Topics: Cryo-electron microscopy and Microscopy

Related papers:

- [Cryo-electron microscopy of vitrified specimens.](#)
- [Electron diffraction of frozen, hydrated protein crystals.](#)
- [Reconstruction of Three Dimensional Structures from Electron Micrographs](#)
- [Electron microscopy of frozen water and aqueous solutions](#)
- [Model for the structure of bacteriorhodopsin based on high-resolution electron cryo-microscopy.](#)

Share this paper:    

View more about this paper here: <https://typeset.io/papers/cryo-electron-microscopy-of-viruses-5gfw37hjef>

Cryo-electron microscopy of viruses

Marc Adrian, Jacques Dubochet, Jean Lepault & Alasdair W. McDowell

European Molecular Biology Laboratory, Postfach 10.2209, D-6900 Heidelberg, FRG

Thin vitrified layers of unfixed, unstained and unsupported virus suspensions can be prepared for observation by cryo-electron microscopy in easily controlled conditions. The viral particles appear free from the kind of damage caused by dehydration, freezing or adsorption to a support that is encountered in preparing biological samples for conventional electron microscopy. Cryo-electron microscopy of vitrified specimens offers possibilities for high resolution observations that compare favourably with any other electron microscopical method.

ALL biological specimens are damaged during preparation for electron microscopy. For particles in suspension, damage is caused by dehydration, adsorption onto the supporting film and by the attempts of the electron microscopist to increase the contrast. Chemical fixation, metal shadowing and negative staining are excellent methods, but they all rely on changing the specimen in order to make it more suitable for observation. As a result electron microscopy has become a highly successful science, but the material observed is generally very different from the original sample.

Cryo-electron microscopy has long been seen as a potential method for preserving the specimen in a state closer to its native state¹. The value of the approach was demonstrated by Taylor and Glaeser², who showed by electron diffraction that the periodic order of frozen-hydrated catalase crystals can be preserved down to less than 3 Å resolution, whereas it is destroyed in air-dried specimens. Another turning point was the discovery that pure water or any aqueous solution can be cooled rapidly enough to prevent formation of ice crystals^{3,4}. Based on this phenomenon, we have developed a simple method for preparing and observing frozen-hydrated specimens from native biological suspensions⁵⁻⁷.

Methodology

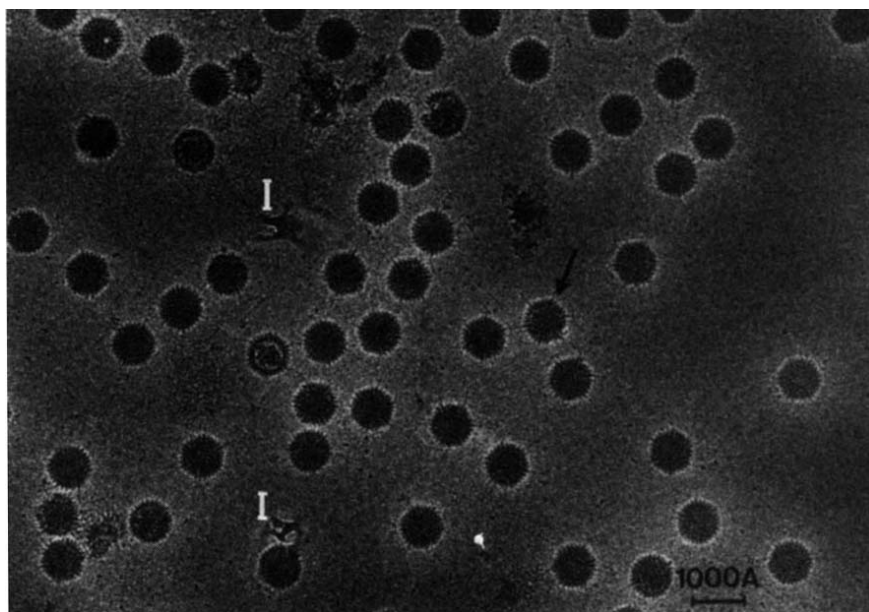
The preparation and observation of frozen-hydrated biological particles involved the following operations: (1) forming a thin layer of the suspension; (2) cooling it into the vitreous state; (3) transferring it into the microscope without rewarming above

the devitrification temperature ($T_d \approx 140$ K); and (4) observing it below T_d and with an electron dose low enough to preserve the structure of the specimen.

As discussed below, all these operations are easy to perform and take about the same time as the very simple negative staining procedure. Apart from the requirement for a cooled specimen holder, operating contamination-free below 140 K, there is no need for special instruments or installation.

The formation of a thin layer of aqueous suspension may initially seem difficult, considering the high surface tension of water, which tends to minimize the surface to volume ratio. This difficulty can be overcome, however, when the appropriate surface property is given to the supporting film^{5,8,9}. A stable thin layer forms readily in the absence of a supporting film when the liquid is stretched over the holes of a hydrophilic surface. In practice, we put a drop of solution on a clean uncoated 200–600-mesh copper specimen-supporting grid, remove most of the liquid with blotting paper and then freeze. On most specimen grids at least some squares are filled with a film of adequate thickness (<3,000 Å). Better results are obtained if the layer is allowed to become thinner by evaporation while being observed under a low-power microscope. The specimen is frozen after a few seconds, when many grid squares have the right thickness. We refer to this method as the 'bare grid method'. Figure 1 shows a specimen of adenovirus prepared in this way. An alternative way of preparation, referred to as the 'perforated film method', consists of mounting the specimen across the holes of a hydrophilic carbon film. As with the bare

Fig. 1 Thin layer of vitrified suspension of unstained and unfixed adenoviruses type 2, prepared by the bare grid method. A 5-μl drop of suspension containing about 5×10^{11} particles per ml in hypotonic solution was put on a clean uncoated 200-mesh copper grid (Science Services, Munich) pretreated by glow discharge in air⁹. The grid was held by a tweezer mounted on a guillotine and was observed with a stereoscopic microscope at $\times 20$ magnification. Most of the liquid was removed by touching the grid edge with a blotting paper. In the next few seconds, evaporation caused the liquid layer, spread over the grid holes, to break. When about half of the grid holes were still filled, the grid was allowed to fall free from a height of 6 cm into a 1.5-cm deep liquid ethane container, cooled close to solidification temperature by liquid nitrogen. The grid was transferred to liquid nitrogen, mounted in a cold stage PW6591/100 (Philips) and rapidly introduced into a Philips 400 electron microscope where it was kept below 110 K during observation. A dozen grid squares were filled with a layer of adequate thickness. Electron diffraction confirmed that the specimen was vitrified. The micrograph was recorded with 80 kV electrons at $\times 12,500$ magnification, with a total dose of $10 \text{ e} \text{Å}^{-2}$ and $\sim 8 \mu\text{m}$ underfocusing. The layer is $\sim 1,200 \text{ Å}$ thick. Note the uniform distribution of the viruses and their well defined shape. The superposition of the upper and lower side of the viruses makes the surface structure difficult to interpret. Spikes are visible in favourable cases (arrow). Ice contaminants on the surface are marked (I).



grid method, a drop of solution is put on the grid and the specimen is frozen immediately after removing most of the liquid with blotting paper. The stabilizing effect of the perforated support ensures that a majority of holes become covered with an adequate layer of suspension. T4 bacteriophages prepared by the perforated film method are shown in Fig. 2.

Vitrification of pure water or dilute aqueous solution is achieved by rapidly cooling the liquid. With layers of less than 1 μm , it is sufficient to immerse the specimen in an efficient cryogen (for example, liquid ethane or propane but not liquid nitrogen⁵). The grid, kept under liquid nitrogen, is then transferred into the cold stage of the microscope which is in turn introduced into the electron microscope. The fact that the specimen is still vitrified in the microscope demonstrates that freezing and transfer have been done correctly.

The nature of amorphous solid water ($\text{H}_2\text{O}_{\text{as}}$) or vitreous ice remains unknown¹⁰. The fact that it can be obtained by rapid cooling of the liquid supports the idea that a continuity of state exists between the liquid and $\text{H}_2\text{O}_{\text{as}}$. The latter should thus be considered as the extreme case of supercooled water. $\text{H}_2\text{O}_{\text{as}}$ is in a metastable state, and devitrifies into cubic ice when it receives enough energy. This is the case when the sample is warmed above the devitrification temperature T_d . At a lower temperature, crystallization may take place under strong electron irradiation⁵, or when mechanical stress is applied¹¹. In the electron microscope, the layer of $\text{H}_2\text{O}_{\text{as}}$ appears as a high viscosity liquid. Particles in a broken vitrified layer can be observed flowing towards an electrically charged corner, where all the material evaporates. Heavily irradiated hydrophobic polystyrene spheres can also be seen to jump out of the film, leaving a hole which soon seals. The total absence of structure presented by a pure $\text{H}_2\text{O}_{\text{as}}$ layer at the resolution considered here is another consequence of its vitreous state. Even the focus-dependent phase contrast graininess produced by any scattering solid cannot be detected. In fact, unless some particles are added to the $\text{H}_2\text{O}_{\text{as}}$ layer, there is no difference between its image and that of a hole, exposed to the same optical density.

The contrast of frozen-hydrated specimens is low, typically three times lower than for freeze-dried specimens. If amplitude contrast only is considered, a 60 Å diameter globular protein is theoretically the smallest that can be detected with an electron dose compatible with beam damage¹². In practice, much smaller structures can be detected, as for example the fibres of the bacteriophage T4 or even DNA molecules (Fig. 2). This is because phase contrast also participates in the image formation and, in fixed beam electron microscopy, is more efficient than amplitude contrast^{13,14}. Unfortunately, the phase contrast information is not transferred equally well for all dimensions. For the large defocusing value ΔF , used in this work, optimal transfer is obtained for dimensions d such as $d^2 = 2\lambda \Delta F / (2n - 1)$, whereas no transfer takes place for $d^2 = \lambda \Delta F / n$. In these equations λ is the wavelength of the electron and n is any integer. For stained specimens it is usual to choose a defocusing value that gives the best phase contrast transfer around 20 Å and to rely on amplitude contrast for much larger dimensions. This method is inadequate for unstained hydrated specimens because it leaves a gap between low resolution amplitude information and high resolution phase information. To bridge this gap, additional micrographs must be recorded with higher defocusing. Such a series may lead to a subjective image of the specimen but a precise quantitative description will require a computer-aided processing of the micrographs (not made in the present work). In Figs 1, 3, 4 and 6a, for example, the strong defocusing reveals the overall aspect of the particles, whereas fine details are revealed in the more sharply focused images of Figs 5 and 6b. The fine details seen in the strongly defocused images must be interpreted with great caution.

Electron beam damage is reduced around liquid nitrogen temperature. The cryoprotection factor, measured by the fading of diffraction points in organic crystals, is about 3 (ref. 7). The maximum dose, D_e , which can be applied without severe damage, depends on the dimension of the structure. For vitrified

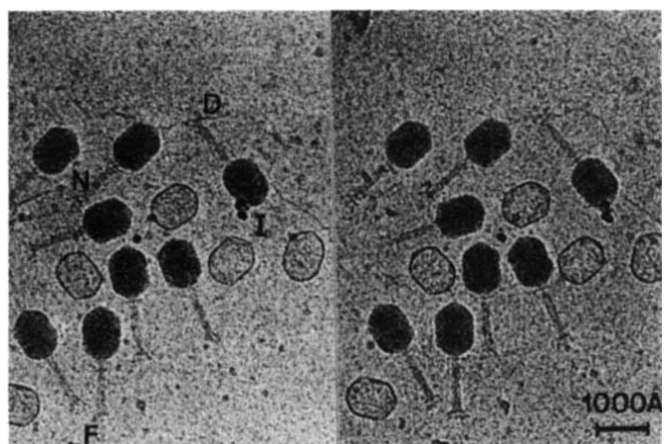


Fig. 2 Stereo view of T4 bacteriophages prepared by the perforated film method. A 5-μl drop of suspension containing about 2×10^{12} particles per ml in water was put on a perforated carbon film³¹ (average diameter of the hole 1.3 μm) mounted on a 200-mesh copper grid and treated by glow discharge in air. The specimen was prepared as for Fig. 1 except that most of the liquid was removed by firmly pressing blotting paper (Whatman; type 1) against the grid for 1 s. The field shown is from a hole of the supporting film. The layer is 1,600 Å thick. Electron optical magnification $\times 12,750$. Tilt angle $\pm 12^\circ$. The figure should be observed through a $\times 2$ magnification stereo viewer. The lower surface of the layer is revealed by contaminating ice crystals (I). The clean upper surface is not discernible. The complete bacteriophages are oriented roughly parallel to the surfaces. Shorter particles, like capsids, tails and needles (N), are more randomly oriented. Tail fibres (F) and DNA (D) are also visible.

catalase crystals it is 40 and 70 e Å⁻² for the reflections corresponding to about 20 and 70 Å, respectively. The phenomenon of bubbling, caused by the hindered escape of volatile molecular fragments induced by the beam⁵, becomes apparent at several tens of electrons per Å². Mass-loss or the effects caused by the flow of water requires an even higher dose. Altogether, this means that high resolution images or even short tilt series can be recorded in good conditions if one of the methods usually used for low dose recording is applied.

The original distribution of the particles is generally well preserved when the unsupported vitrified layer of suspension is much thicker than the particles. The latter are then randomly positioned within the layer. When the thickness of the layer is close to the dimension of the particles, the interaction with the surface becomes noticeable. Hydrophobic polystyrene spheres tend to come out onto the surface whereas hydrophilic viruses avoid the surface by leaving the thinnest regions (adenovirus) or by orienting their long axis in a plane parallel to the surface (vesicular stomatitis virus, T4). An example is shown in the stereo view of Fig. 2.

In principle, an aqueous suspension with any concentration of solute can be used to prepare frozen-hydrated specimens. A high concentration of sugar or glycerol, or a viscous suspension, does not disturb the preparation, but a high salt concentration (>1 M) leads, in some cases, to a grainy appearance. This may be due to a rearrangement of the material during freezing or to the effect of low dose irradiation. By changing the density of the solution, solutes also change the contrast of the particles. Furthermore, because some drying takes place before freezing, especially when the bare grid method is used, the final concentration of solute in the vitrified state may be significantly higher than in the original suspension. Note also that, because the particles cannot adsorb to a supporting film, and because the total volume of observed material is small, the original concentration of the particles must be high.

The excellent preservation of the particle shape is obvious in Figs 1 and 2. Figure 3 shows a vitrified preparation of the very labile preheads of bacteriophage T4, unfixed in the high-salt

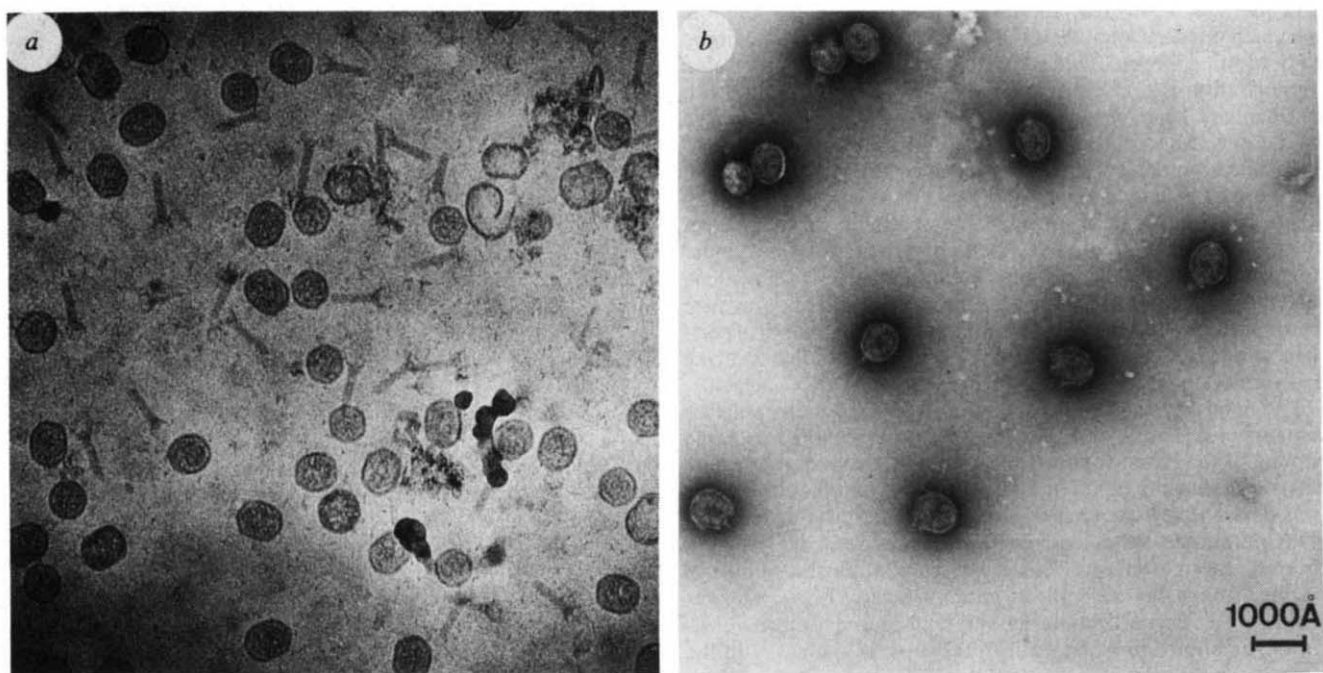


Fig. 3 Preheads of T4 bacteriophage. *a*, The prehead formed by the mutant 21⁻ and extracted by chloroform lysis in 0.5 M NaCl and one run of low speed centrifugation was prepared by the perforated film method. Electron optical magnification $\times 25,000$. The preparation shown in *b* (courtesy of B. Keller) was obtained from 21 ts mutants, fixed in 1% glutaraldehyde and further purified on a glycerol gradient. It was prepared for electron microscopy by negative staining with 2% sodium phosphotungstate. Electron optical magnification $\times 20,000$.

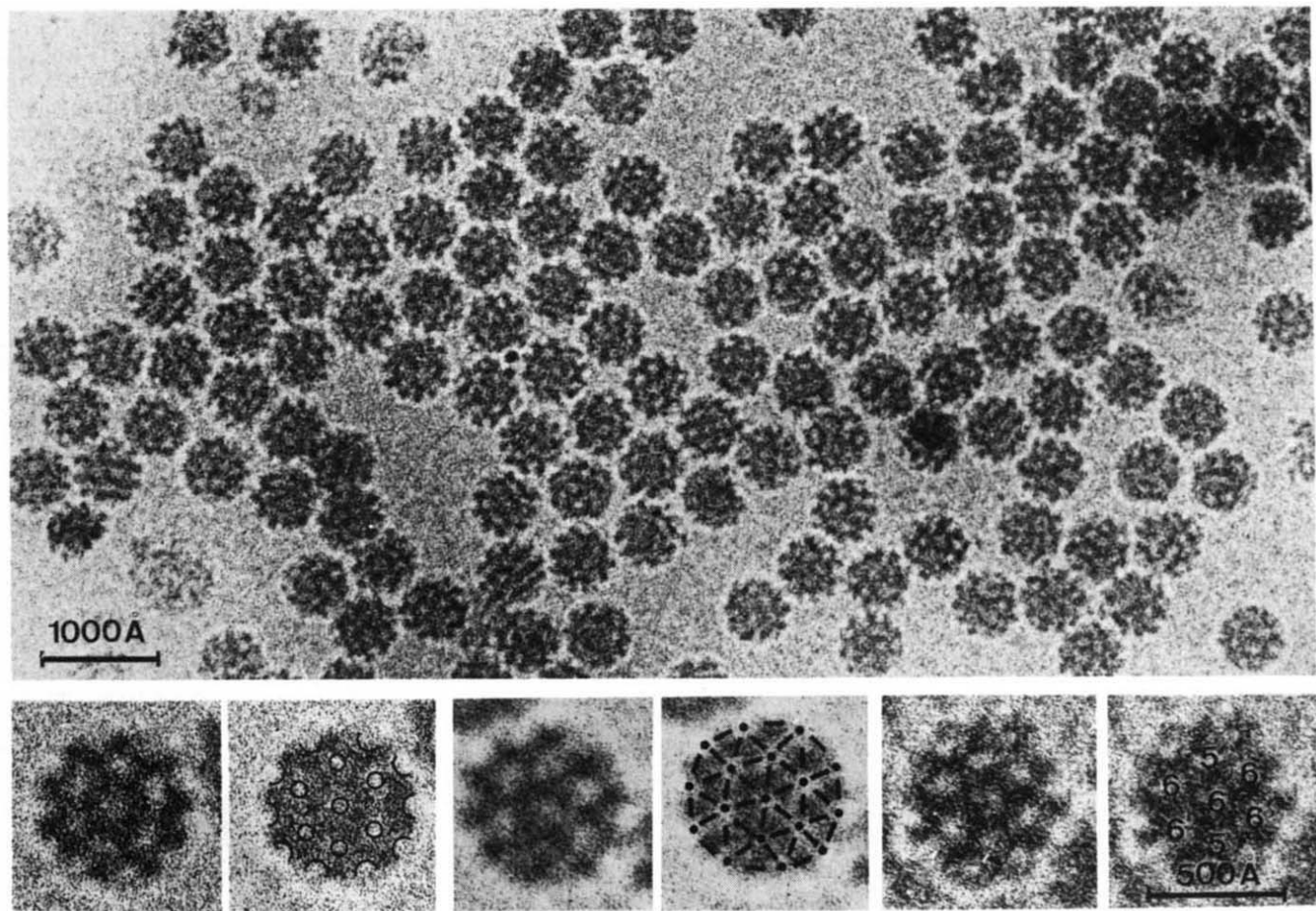


Fig. 4 Semliki Forest viruses prepared by the perforated film method. A suspension containing ~ 5 mg protein per ml in 50 mM Tris, 100 mM NaCl³², was prepared as for Fig. 2. Electron optical magnification $\times 15,000$. Underfocusing, 3.5 μm . Three selected images of virions projected along their 2-fold axis are shown at higher magnification. They are underfocused by 6–9 μm . Each image is duplicated and superimposed with the schematic outline of the structure, the triangular network, or a designation of the 5- and 6-fold low density nodes.

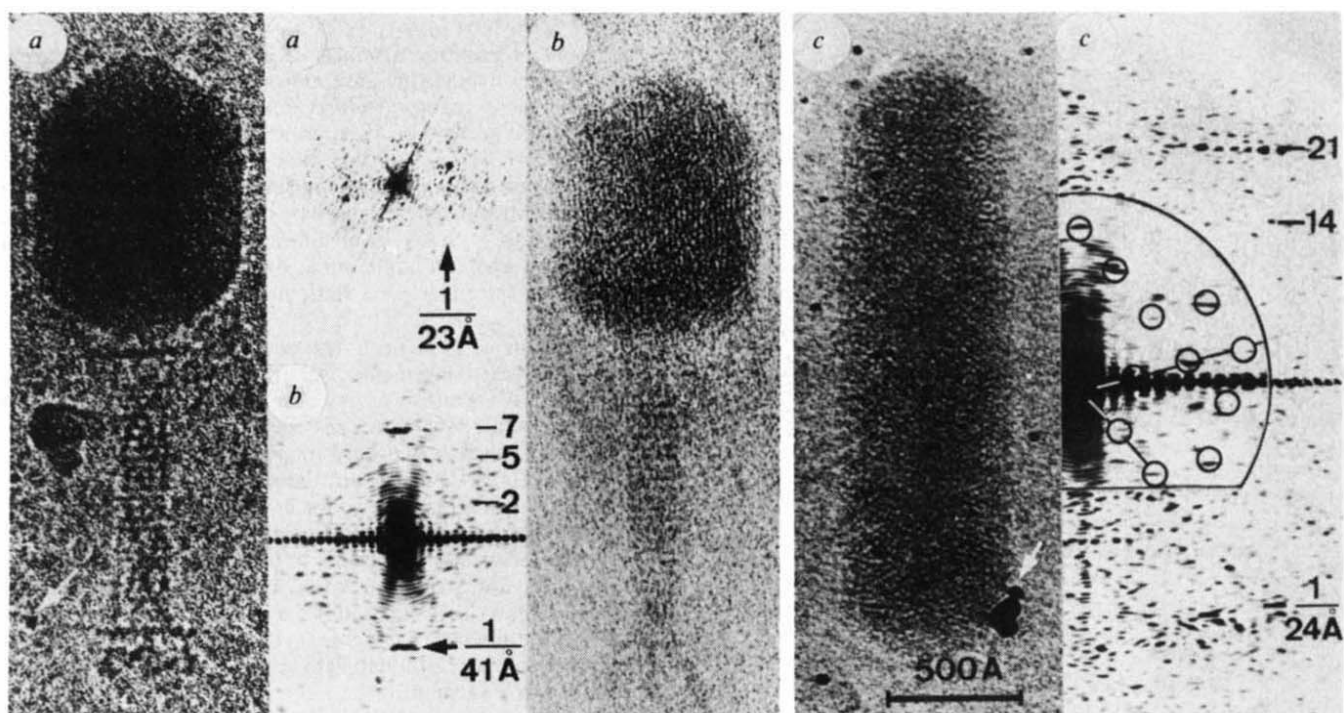


Fig. 5 T4 and CbK bacteriophages mounted on carbon films pretreated by glow discharge in pentylamine⁵. In all three micrographs the thickness of the vitrified layer is greater than that of the virus. Electron magnification $\times 42,000$. Dark spots (arrows) are gold particles deposited on the supporting film as focusing aids. The micrographs were underfocused by: *a*, $2.5 \mu\text{m}$; *b*, $0.5 \mu\text{m}$; *c*, $1.2 \mu\text{m}$. The T4 tail structure is best seen in *a*, whereas the head structure is seen in *b*. The structure in the head of the bacteriophage CbK (*c*) is characterized in its optical diffractogram by a pair of strong reflections at $1/24 \text{ \AA}$. The central part of the diffractogram originates from a strongly underfocused micrograph (not shown). It shows the reflections due to the helical structure of the capsid. Those corresponding to one side are circled. The 14th and 21st layer lines are marked.

extraction medium (Fig. 3*a*), and fixed and desalinated for the negatively stained preparation (Fig. 3*b*). Other examples of good preservation are that polyheads of the bacteriophages T4 are not flattened and the tails of the bacteriophages λ are straight.

The dimensions of the particles in the frozen-hydrated state are close to their dimensions in liquid solution. Diameters for adenovirus, λ bacteriophage and the isometric head of T4 bacteriophage are 860 ± 30 , 630 ± 20 and $850 \pm 20 \text{ \AA}$, respectively. These values agree well with the reported respective low angle X-ray diffraction measurements of 840 (ref. 15), 640 (ref. 16) and 850 \AA (ref. 17). A more precise comparison can be made on organic crystals. For catalase crystals, the lattice parameters determined in water at room temperature by X-ray diffraction¹⁸ are, within 1% measurement error, identical with those measured in vitreous ice, taking ice crystals as calibration standard. This excellent agreement is surprising, as pure $\text{H}_2\text{O}_{\text{as}}$ has a 5–7% smaller density than liquid water at room temperature⁶ and would therefore be expected to expand by about 2% on vitrification. In this case also, vitrified water seems to behave like a liquid around the more rigid biological particles.

Virus structure

The structure of Semliki Forest virus remains controversial. Electron microscopical evidence obtained on negatively stained preparations suggests, although with some ambiguity, that the envelope is icosahedral with a triangulation number $T = 4$ (ref. 19). Biochemical evidence associated with independent determination of the total mass of the virion seems incompatible with this value and suggests $T = 3$ (ref. 20). As can be seen in Fig. 4, the geometry of the envelope of the Semliki Forest virus is clearly visible in frozen hydrated specimens. Because of the superposition of the two sides of the particle, only those viruses which are observed along their 2-fold axis are easy to interpret

in projection. When this is the case, two 5-fold low density nodes on the opposite sides of the 6-fold central low density node are generally visible. This configuration is the unmistakable signature of $T = 4$.

The prolate icosahedral capsid of the T4 bacteriophage is formed by two opposed caps with triangulation number $T = 13$, joined by a quasi-cylindrical segment characterized by its Q number^{21–23}. The ratio, R , of the length to the width of the capsid is directly related to Q . R varies by ~3% for two successive values of Q . Because of distortion during conventional specimen preparation, the value of R could not, until now, be measured accurately. When measured on micrographs similar to that of Fig. 2, R is found to be 1.431 ± 0.024 . In principle this accuracy should be sufficient to determine Q without ambiguity. We tentatively confirm the previously suggested²⁴ value of $Q = 21$ and will report elsewhere (U. Aebi, J.D., E. Kellenberger, J. Lepault and M. Wurtz, in preparation) the detailed method for measuring R and for calculating its relation to Q , taking into account that capsomeres in the caps are bent differently from those in the quasi-cylindrical segment.

High-resolution observations can also be made of frozen hydrated viruses. The structure of the tail of bacteriophage T4 is clearly revealed in Fig. 5*a*. Its diffractogram is characterized by a strong meridional reflection on the 7th layer line, corresponding to 41 \AA , and by strong intensities on the 2nd and 5th layer lines. This agrees with results obtained previously on negatively stained images^{25,26}. The arrangement of the DNA in the intact T4 head is more clearly visible than in previous studies. In addition to the pattern of concentric ellipses already described^{27,28}, some heads show a pattern of parallel lines separated by about 23 \AA and oriented along the long axis of the head (Fig. 5*b*). In the elongated head of bacteriophage CbK, the previously undetected periodic structure of the material inside the capsid is responsible for the characteristic aspect of the image and for the strongest reflections of the optical

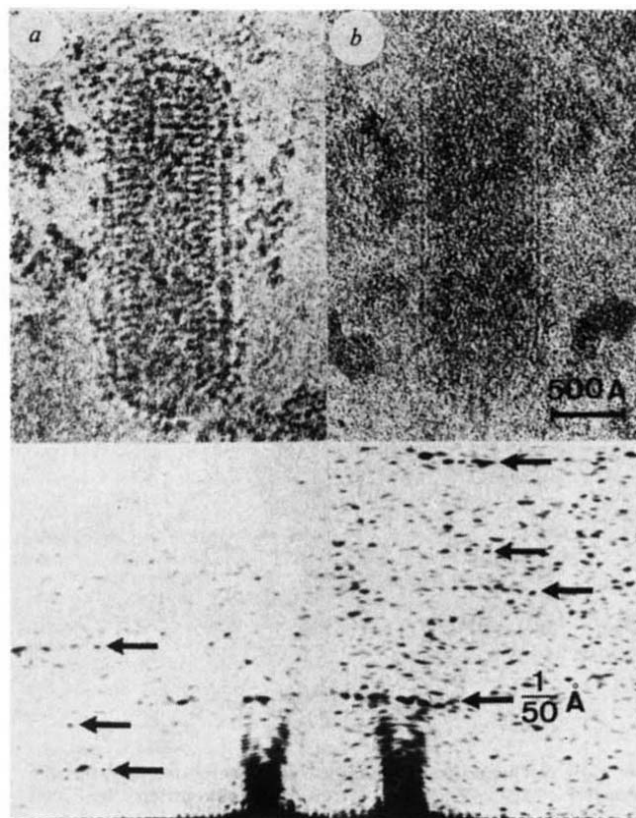


Fig. 6 Vesicular stomatitis viruses prepared by the perforated film method. Electron optical magnification $\times 43,000$. The micrographs were underfocused by: *a*, $4 \mu\text{m}$; *b*, $0.7 \mu\text{m}$. The reflections which are found to be relevant, when other micrographs are also considered, are marked in the diffractograms.

diffractogram (Fig. 5c), and corresponds to a distance of $\sim 24 \text{ \AA}$ along the head axis. The lattice constant of the capsid is about 120 \AA^{29} . In frozen hydrated specimens, it is visible in strongly defocused images.

The general aspect of vesicular stomatitis virus is seen in the strongly underfocused image of Fig. 6*a*, whereas the fine structure is better revealed in Fig. 6*b*, which is more sharply focused. The optical diffractogram reveals many more reflections than the previously observed 50 \AA periodicity³⁰. Their interpretation must take into account the fact that the virus appears polymorphic, probably because most of the particles are partially degraded.

Received 8 August; accepted 21 October 1983.

1. Fernandez-Moran, H. *Expl Cell Res.* **3**, 282–350 (1952).
2. Taylor, K. A. & Glaeser, R. M. *Science* **186**, 1036–1037 (1974).
3. Brüggeler, P. & Mayer, E. *Nature* **288**, 569–571 (1980).
4. Dubochet, J. & McDowall, A. W. *J. Microsc.* **124**, RP 3–4 (1981).
5. Dubochet, J., Lepault, J., Freeman, R., Berriman, J. A. & Homo, J.-Cl. *J. Microsc.* **128**, 219–237 (1982).
6. Dubochet, J., Chang, J.-J., Freeman, R., Lepault, J. & McDowall, A. W. *Ultramicroscopy* **10**, 55–62 (1982).
7. Lepault, J., Booy, F. P. & Dubochet, J. *J. Microsc.* **129**, 89–102 (1983).
8. Hayward, S. B., Grano, D. A., Glaeser, R. M. & Fischer, K. A. *Proc. natn. Acad. Sci. U.S.A.* **75**, 4320–4324 (1978).
9. Dubochet, J., Groom, M. & Müller-Neuteboom, S. in *Advances in Optical and Electron Microscopy* Vol. 8 (eds Cosslett, V. E. & Barer, R.) 107–135 (Academic, London, 1982).
10. Angell, C. A. *A. Rev. phys. Chem.* **34**, 593–630 (1983).
11. Chang, J.-J. *et al.* *J. Microsc.* **132**, 109–123 (1983).
12. McDowall, A. W. *et al.* *J. Microsc.* **131**, 1–9 (1983).
13. Erickson, H. P. & Klug, A. *Phil. Trans. R. Soc. B261*, 105–118 (1971).
14. Lepault, J. & Pitt, T. *EMBO J.* **3**, 101–105 (1984).
15. Devaux, C., Timmins, P. A. & Berthet-Colominas, C. *J. molec. Biol.* **167**, 119–132 (1983).
16. Earnshaw, W. C., Hendrix, R. & King, J. *J. molec. Biol.* **134**, 575–594 (1979).
17. Earnshaw, W. C., King, J. & Eislerling, F. A. *J. molec. Biol.* **122**, 247–253 (1978).
18. Unwin, P. N. T. *J. molec. Biol.* **90**, 235–242 (1975).
19. Söderlund, H. von Bonsdorff, C.-H. & Ulmanen, I. *J. gen. Virol.* **45**, 15–26 (1979).
20. Simons, K. & Warren, G. *Adv. Protein Chem.* **36**, 79–139 (1983).
21. Moody, M. F. *Virology* **26**, 567–576 (1965).
22. Aeby, U. *et al.* *J. supramolec. Struct.* **2**, 253–275 (1974).
23. Branton, D. & Klug, A. *J. molec. Biol.* **92**, 559–565 (1975).
24. Eislerling, F. A. in *The Bacteriophage T4* (eds Mathews, C. K., Kutter, E. M., Mosig, G. & Berget, P. B.) 11–24 (Am. Soc. Microbiol., Washington DC, 1983).
25. Amos, L. A. & Klug, A. *J. molec. Biol.* **99**, 51–75 (1975).
26. Smith, P. R., Aeby, U., Josephs, R. & Kessel, M. *J. molec. Biol.* **106**, 243–275 (1976).
27. Richards, K. E., Williams, R. C. & Calendar, R. *J. molec. Biol.* **78**, 255–259 (1973).
28. Earnshaw, W. C., King, J., Harrison, S. C. & Eislerling, F. A. *Cell* **14**, 559–568 (1978).
29. Leonard, K. R., Kleinschmidt, A. K., Agabian-Keshishian, N., Shapiro, L. & Maizel, J. V. Jr *J. molec. Biol.* **71**, 201–206 (1972).
30. Cartwright, B., Smale, C. J., Brown, F. & Hull, R. *J. Virol.* **10**, 256–260 (1972).
31. Fukami, A. & Adachi, K. *J. Electron Microsc.* **14**, 112–118 (1965).
32. Kääriäinen, L., Simons, K. & von Bonsdorff, C.-H. *Annls Med. exp. Biol. Fenn.* **47**, 235–248 (1969).

Conclusion

The usual preparation artefacts of electron microscopy seem to be largely avoided in unsupported vitreous specimens—in particular there are no artefacts due to staining, fixation and adsorption. It seems also that the thin layer of suspension is a representative sample of the bulk material, although there remains the existence of long-range interactions with the surface and a concentration effect caused by partial drying before freezing. Although at some level differences must exist between the vitreous and the liquid state, our observations show that the vitreous state is a good static model of the liquid suspension.

Fine details of biological structures are clearly revealed in frozen-hydrated specimens. All the structures previously described in the viruses we have observed have also been shown in frozen-hydrated specimens and several other important structures have been revealed here for the first time. This demonstrates once more that it is not the signal produced by a given structure which is important, but its signal-to-noise ratio. The disadvantage of the low contrast presented by frozen-hydrated specimens seems, in many cases, to be more than compensated for by their low structural noise. In particular, the reduced distortion allows us to take more advantage of periodic structures and the absence of structure in the supporting water makes the particles appear—though with low contrast—as if they were suspended in a vacuum.

Future work to establish the potential of this new electron microscopy technique should take account of the following points: (1) Water molecules seem to be mobile under the electron beam. Small molecules in solution or even biological structures could also be rearranged. This is surely the case for the molecular fragments causing bubbling. Preliminary evidence suggests that this may also be the case at low dose in concentrated salt solution. The extent to which the vitreous material can still be regarded as a static model of the liquid should be explored. (2) In some instances, the upper and lower side of a particle, in an unsupported layer, do not appear symmetrical. It is possible that the contrast may be influenced by interaction with the surfaces. (3) A strong positive staining effect occurs with biological particles when a low concentration of heavy metal salts is added to the liquid solution. Exploiting this possibility for increasing contrast could be useful in complementing the study of unstained material.

We thank Sir John Kendrew for his support during the long initial period of this research, and the following people for useful discussions and the gift of biological material: Drs U. Aeby, W. Baschong, C.-H. v. Bonsdorff, J. Caldentey, E. Kellenberger, B. Keller, K. R. Leonard, L. Philipson, V. Pirrotta, A. C. Steven, J. Tooze and M. Wurtz.